applied sciences

MDPI

Article

New Candidate Multicomponent Chalcogenide Glasses for Supercontinuum Generation

Claudia Goncalves [1,†], Myungkoo Kang [1,†], Byoung-Uk Sohn [2], Gufan Yin [3], Juejun Hu [3], Dawn T. H. Tan [2] and Kathleen Richardson [1,*]

1 CREOL, College of Optics and Photonics, University of Central Florida, Orlando, FL 32816, USA; claudia.goncalves@ucf.edu (C.G.); myungkoo@creol.ucf.edu (M.K.)
2 Photonics Devices and Systems Group, Singapore University of Technology and Design, 8 Somapah Rd. Singapore 487372, Singapore; byounguk_sohn@sutd.edu.sg (B.-U.S.); dawn_tan@sutd.edu.sg (D.T.H.T.)
3 Department of Materials Science and Engineering, Massachusetts Institute of Technology, Cambridge, MA 02139, USA; gyin@mit.edu (G.Y.); hujuejun@mit.edu (J.H.)
* Correspondence: kcr@creol.ucf.edu
† These authors contributed equally to this work.

Received: 2 October 2018; Accepted: 23 October 2018; Published: 28 October 2018

Abstract: Broadband supercontinuum (SC) generation requires host material attributes defined by both optical and physical properties and the material's manufacturability. We review and define the trade-offs in these attributes as applied to fiber or planar film applications based on homogeneous glass property data, and provide a series of examples of how one might optimize such attributes through material compositional and morphology design. As an example, we highlight the role of varying composition, microstructure, and linear/nonlinear optical properties, such as transmittance, refractive index, and the multiphoton absorption coefficient, for a series of novel multicomponent chalcogenide glasses within a model $GeSe_2$-As_2Se_3-PbSe (GAP-Se) system. We report key optical property variation as a function of composition and form, and discuss how such glasses, suitable for both fiber and planar film processing, could lend themselves as candidates for use in SC generation. We demonstrate the impact of starting glass composition and morphology and illustrate how tailoring composition and form (bulk versus film) leads to significant variation in linear, nonlinear, and dispersive optical property behavior within this system that enables design options that are attractive to optimization of desirable SC performance, based on optical composites.

Keywords: photonics; supercontinuum generation; nonlinear optics; infrared optical materials; chalcogenide glass science

1. Introduction

Broadband infrared (IR) supercontinuum (SC) light sources have gained tremendous interest in the last decade, due to their potential use in a variety of telecommunication, sensing [1], lasing, and defense-related applications [2,3]. Most important for consideration of use in SC applications are material attributes related to the medium's optical properties, including transmission window related to pump wavelength and spectral window of use, linear and nonlinear refractive indices, material dispersion, zero-dispersion wavelength, and single/multi-photon absorption behavior. As high intensity material response is also important, further consideration as to the likelihood of photo-structural modification, laser damage resistance, and other physical properties influenced by thermal effects (thermo-mechanical robustness, coefficient of thermal expansion (CTE), and environmental stability) is necessary. Lastly, the final form of the SC material requires attention to specific manufacturing-related material behavior to achieve the final form of the SC component/device

(film deposition behavior and fiber drawing attributes such as viscosity temperature behavior and multi-material compatibility). As can be seen, such a material performance checklist extends beyond the typical optical property criteria that evaluates candidate materials only based on their linear and nonlinear refractive indices and low optical loss in the mid- and long-wave IR (MWIR and LWIR, respectively) [3]. The investigation of these properties has largely focused on candidate glass materials in bulk (three-dimensional, 3-D) and fiber (one-dimensional, 1-D) geometries [4–28]. Additionally, intermediate geometries, such as bulk planar disks (two-and-a-half-dimensional, 2.5-D) and thin films (two-dimensional, 2-D), have been discussed as attractive for photonic device integration where on-chip sources are desired for multispectral sensing and detection applications [4–6]. Furthermore, the availability of candidate SC materials suitable for broadband use in such planar forms would enable expanded understanding of chemistry/structure/property/form behavior across a spectrum of material dimensions providing insight into ideal geometries, performance limitations, and optimal property potential, for specific applications.

To date, IR transparent candidates for SC have largely relied on existing, commercially available materials with known (finite and unoptimized for the application) physical property attributes. Operating in a regime of anomalous dispersion ensures that nonlinear effects including cascaded four wave mixing and soliton fission may occur. These effects are favorable for extending the supercontinuum bandwidth. Similarly, maximizing the optical nonlinearity of the medium ensures that a supercontinuum can be efficiently generated at lower powers. Strategies to maximize the optical nonlinearity while maintaining broadband operability include: (1) geometric engineering of the fiber/waveguide to maximize the nonlinear parameter, and (2) utilizing material platforms with large intrinsic nonlinearities. From a material standpoint, most efforts to date have focused on increasing the optical nonlinearity of homogeneous glasses, characterized in bulk, fiber, or waveguide form [29–35]. Non-oxide glasses' transmission typically extend well beyond the intrinsic multi-phonon absorption edge of oxides (silicates, phosphates, and tellurites), and thus, are more suited for truly broadband IR (defined here as being near-IR, MWIR, and LWIR transmissive).

Chalcogenide (ChG) glasses are superb candidates for SC applications, due to their high linear refractive indices (between 2.2 and 2.6 for sulfide, 2.4 and 3.0 for selenide, and 2.6 and 3.5 for telluride glasses [24]), low phonon energies, and high optical nonlinearity (typically ~500 times more than traditional silica glasses [25]) attributable to the low vibrational energies of molecular bonds dictated by heavy, chalcogen atoms. The optical transparency of ChGs can extend from the visible up to 10 μm for sulfides, 12–13 μm for selenides, and 20 μm for tellurides [23–25], making them suitable as fibers and waveguides for use in a wide range of infrared optical applications. The first studies on chalcogenide fibers in the mid-1980s reported high optical losses due to impurity absorption, which was a major limiting factor [36,37]. With the development of low-loss chalcogenide fibers, SC sources that generate light in the MWIR (3–8 μm) and LWIR (8–14 μm) spectral regions gradually attracted further interest. In particular, experimental work on chalcogenide fibers for SC generation first focused on binary As_2S_3 fibers, where a spectrum from 2–4.6 μm was demonstrated in an As_2S_3 step-index fiber [38,39]. Since then, efforts to realize broad SC generation in MWIR using multi-component chalcogenide fibers have been also made. For example, different chalcogenide compositions such as Ge-As-Se, Ge-Sb-Se, and Ge-As exhibited ultra-broadband SC generation at 2–12 μm [15,40–45]. In addition to fibers, chalcogenide on-chip waveguides have also been established as a major platform for SC generation. Waveguides provide greater flexibility in dispersion engineering compared to fibers; the ability to engineer the zero-dispersion wavelength to be very close to the pump wavelength greatly facilitates the generation of supercontinuum [46]. One of the earliest demonstrations of broadband SC generation at the MWIR was reported to show transparency up to 8 μm [33], and a variety of compositions, such as Ge-Sb-S, Ge-Te-Sb, and As_2S_3, have since been developed as waveguides to show broadband SC generation [33,47–49]. Early demonstrations of chalcogenide waveguide-based SC generation were achieved using pumps located at the telecommunications wavelength [47–49]. Most recently, chalcogenide waveguides have been fully leveraged for their transparency far into the

mid-long infrared wavelengths for SC generation [50]. Chalcogenide waveguides pumped at ~4 μm have been demonstrated to span from 2 μm to >10 μm [34], thus further leveraging the chalcogenide glass' optical transparency into the far-infrared. As shown in these examples, such properties can be engineered through composition tailoring, as in the case of one well-studied bulk ChG glass system, where the nonlinear refractive index of Ge-Sb-Se has been correlated with composition, and shown to increase with the concentration of Sb [7] as well as Se [18]. Chalcogen substitution of Se by S in simple binary $As_{40}Se_{60}$ has been shown to lead to an increase in nonlinear refractive index of the glass at the expense of increased multiphoton absorption [22]. Furthermore, as one might expect, with the addition of highly polarizable glass constituents, an increase in the concentration of Te in Ge-As-Se-Te glasses has also been shown to increase glass' nonlinearity [51].

Since properties of a glass are strongly dependent upon its thermal history during fabrication, glass in fiber and film form often has optical properties different from those of their bulk counterpart. This variation is caused by processing conditions (imparting variations in material thermal history) to the final component form, and requires consideration in the design and fabrication of SC structures in planar (thin bulk or films) or fiber form, as key properties may vary from those reported for bulk glasses. Most studies to date on this topic have been dedicated to measurement of the optical nonlinearity of fibers made of single ChG material [2,8–10], while other special geometries, such as micro-structured optical fibers [11–13] and refractive index-graded fibers [14,15], have been investigated more recently. Extensively studied are simple binary ChGs, such as As_2S_3 and As_2Se_3 fibers, reported to show high nonlinear refractive indices as characterized in the near-IR and MWIR spectral region [16–19]. These materials have potential to enable broad spectral emission suitable for use as a source; however, detailed optical material property data have largely not extended past the MWIR, where most labs routinely characterize such properties. While an optimal material would need to be transmissive over a broad spectral range and have tailorable linear and nonlinear refractive indices as well as composition-tailorable dispersion behavior, the extension of any generated SC to wavelengths needs to be close to the material's band-edge, or more importantly, into the deep sub-bandgap region. This region is especially important for potential photo-induced material modification, as both linear and nonlinear absorption increases near the band edge. This, as reported for As_2S_3 and other glass systems [52,53], can lead to deleterious effects such as photo-structural modification where light is sufficiently energetic to cause bond re-arrangement thereby modifying or significantly altering desirable optical properties. As the mechanism of SC requires high pump intensities coupled with high host optical nonlinearity, broad spectral window, and suitable laser damage resistance at the high(er) powers needed to induce the optical nonlinearity, intensity-dependent performance combined with knowledge of fabrication flexibility and thermal stability is key to defining suitable SC candidate materials [2,20].

In addition to the optical property merits of ChG glasses, their high viscoelasticity enables easy shaping to reduced dimensions such as fiber and thin film geometries that can be integrated into photonic devices [14,20]. Ideally, these devices require a high nonlinear figure of merit (FOM = $n_2/(\lambda I^{m-2}\alpha_{nPA})$, where n_2 is the nonlinear refractive index, λ is the wavelength, I is the laser pump power, and α_{nPA} is the multiphoton absorption coefficient, respectively) [26]. This FOM trades off wavelength-specific nonlinearities with undesirable nonlinear loss, providing a guide for expected material performance. As noted, this is often hard to calculate, as data is often only measured at a single wavelength, not across the spectrum enabled by the broadband material. Compositional tuning is one way to engineer the optical properties of ChGs; however, such engineering does not always include consideration of other physical properties important for manufacturability, and ultimately, the usage environment. In this paper, we review prior efforts to engineer optical properties via compositional tuning (only) in homogeneous glasses; we further extend these findings to present the potential for SC property enhancement through microstructural modification (i.e., selective conversion of a glass to a glass ceramic). Formation of such an optical composite offers parallel opportunities for both optical property-tailoring (linear and nonlinear refractive indices and optical dispersion) combined

with improvements to thermal, mechanical [54,55], and chemical stability critical for optimizing in-use performance [56,57].

To illustrate the potential to leverage optical and physical property engineering where multi-spectral data is being compiled, we examined the property tailoring enabled in a model glass system recently investigated for the creation of optical nanocomposites, specifically multiple compositions within the multicomponent $GeSe_2$-As_2Se_3-PbSe (GAP-Se) system. While not exclusive to the application of SC generation, this glass system illustrates how morphology and microstructural tailoring with a secondary phase of known chemistry, refractive index, size, and size distribution can result in composites with broadly tailorable linear and nonlinear optical and physical properties within a narrow composition space. GAP-Se materials have recently been shown to exhibit desirable transparency over a wide range of wavelengths from 1 to 12 μm, high linear/nonlinear refractive indices, and expansive property tunability via composition alloying and microstructural tailoring [56–66]. However, like most covalently-bonded ChG made from large ions, weak(er) bonding (as compared to oxides) can lead to reduced thermal/mechanical properties, photosensitivity when pumped with near bandgap light, and low(er) laser damage resistance at the benefit of broad IR transparency [19,27].

Following a short review of the state-of-the-art understanding of key optical properties requisite for SC applications, we present examples highlighting the novelty and scalability of our approach based upon planar bulk and film forms of GAP-Se glasses. We discuss where our model system stands in terms of their attributes compared to other material systems as an example to exploit performance optimization for potential use in planar SC applications.

2. Optical and Physical Properties and Composition: Glasses

SC generation requires candidate materials to possess high linear and nonlinear refractive indices without appreciable optical degradation such as scattering and absorption losses [3]. Traditional homogeneous glasses have fixed values of properties that usually vary systematically with composition, with heavier, more polarizable species leading to higher linear and nonlinear properties. Losses are often caused by impurities in the parent host; however, these can also be related to nanoscale crystallization and interfacial defects, such as those seen in core/clad fibers of dissimilar refractive index, trapped inclusions or bubbles, or sidewall roughness such as that seen in planar waveguides or resonators [67], which can lead to scattering losses. While SC spectral width is typically defined by the host's transmission window, refractive index, and dispersion, broadband materials can suffer from laser damage induced by high intensity pump radiation in lossy structures [19,51,68–73]. This damage can surface in nature in fibers (at end-faces or cleaved interfaces) or intrinsic within the bulk material due to impurities, inhomogeneities, or other defects. Homogeneous glass refractive index data and surface/bulk laser damage thresholds and mechanisms in ChGs are not widely reported in the MWIR and LWIR regions; where reported, typically measurements have been made in the band-edge region of most ChGs, near 1 μm with CW or long-pulse (low intensity) regimes. Representative literature data useful for assessing suitability of glass composition for SC applications is summarized for a diverse range of IR transparent glasses in Table 1 [7,19–21,26,28,51,54,56,58–60,74–77].

Included for comparison in Table 1 is data on glass(es), where reported, in bulk and film form measured at various IR wavelengths. As can be seen, the thermal history associated with the processing method used to create the film (or fiber) into its final form can impart a unique and variable structure to the resulting material. This structural variation for a constant composition has been shown to impact linear and nonlinear properties, and was first highlighted in [28]. Such structural variations are attributable to subtle variation in composition, bonding, and thus density, and polarizability, imparting refractive indices that can be processing method-specific. Additionally, since full dispersion data across the IR spectral window of SC generation is often difficult to measure, the properties available to model component behavior is often limited to data at a single wavelength. Hence, complete dispersion behavior is a desirable knob for optimization of material choice, and should

be quantified [20]. For comparison to previously reported data in Table 1, the linear refractive index collected from GAP-Se bulk and films are noticeably greater than those reported for more simple binary or ternary compositions, impacted by the addition of Pb. Furthermore, Ge, which has been often used for nonlinear optical applications, has a nonlinear refractive index of 4.57×10^{-5} cm^2/GW and a three-photon absorption coefficient of 1.027 cm^3/GW^2 at 4.5 µm [78], which are greater than those of GAP-Se glasses. However, the high nonlinear absorption for Ge could be a limitation on the purpose of all optical switching. Therefore, a trade-off between high n_2 and low nonlinear absorption is strongly desired and requires the development of new candidate materials, such as GAP-Se glasses reported in this study. It should be noted that full broadband nonlinear property characterization of GAP-Se films in both their as-deposited amorphous and converted glass ceramic form, is ongoing.

Table 1. Linear and nonlinear optical parameters of bulk and film chalcogenide (ChG) glasses measured at the wavelengths shown.

Form	Composition (mol%)	n_1 at (λ)	λ = 1.06 µm		λ = 1.55 µm		Ref
			n_2 ($\times 10^{-15}$ cm^2/W)	α_2 (cm/GW)	n_2 ($\times 10^{-15}$ cm^2/W)	α_2 (cm/GW)	
Bulk	$As_{40}Se_{60}$	2.38 (1.33 µm)			4		28
	$As_{40}S_{40}Se_{20}$	2.47 (1.33 µm)			8	<0.01	28
	$As_{24}S_{38}Se_{38}$	2.32 (1.33 µm)	15 (1.3 µm)	0.06	17.5	<0.05	28
	$Ge_{30}As_{11}Se_{49}Te_{10}$	2.50 (1.33 µm)	14 (1.3 µm)	0.4	11	0.16	28
	$As_{30}Se_{63}Sb_4Sn_3$	2.80 (1.33 µm)		0.52	10	0.17	28
	$Ge_{20}Se_{80}$				0.372	6.01×10^{-6}	7
	$Ge_{20}Sb_5Se_{75}$				0.429	3.14×10^{-6}	7
	$Ge_{20}Sb_{10}Se_{70}$				0.622	4.78×10^{-6}	7
	$As_{40}Se_{60}$				1	16×10^{-6}	7
	$As_{40}S_{60}$	2.430 (1.55 µm)	35 (1.35 µm)		28.5		26,51
	$Ge_{11.5}As_{24}Se_{64.5}$	2.634 (1.55 µm)	88.3 (1.35 µm)		79		26
	$Ge_{15}Sb_{10}Se_{75}$	2.598 (1.55 µm)	76.7 (1.35 µm)		7.5		26
	$Ge_{15}Sb_{15}Se_{70}$	2.690 (1.55 µm)	137 (1.35 µm)		10		26
	$Ge_{20}Se_{80}$		1.3				74
	$GeSe_6$		1.7				74
	$Ge_{11}As_{11}Se_{78}$		2.2				51,74
	$Ge_{10}As_{10}Se_{70}Te_{10}$		1.9				51
	$Ge_{10}As_{10}Se_{60}Te_{20}$		2.0				51
	$(GeSe_2)_{90}(Sb_2Se_3)_{10}$	2.51 (1.064 µm)	8.9	10.7			21
	$(GeSe_2)_{60}(Sb_2Se_3)_{40}$	2.85 (1.064 µm)	14.8	12.4			21
	$(GeSe_2)_{40}(Sb_2Se_3)_{60}$	2.51 (1.064 µm)	21.2	21.5			21
	$(GeSe_4)_{0.5}(AsSe_3)_{0.5}$		2.2	2.7			19
	$GeAs_2Se_3$		1.85	5.9			19
	$Ge_{10}As_{10}Se_{80}$		2.2				75
	$Ge_{10}As_{20}Se_{70}$		1.40				75
	$Ge_{20}As_{40}Se_{40}$		1.85				75
	Composition (mol%)	n_1 at λ = 4.515 µm	n_2 at λ = 4.515 µm ($\times 10^{-15}$ cm^2/W)		α_2 at λ = 4.515 µm ($\times 10^{-3}$ cm^5/W^3)		Ref
	$GeSe_2$-As_2Se_3-PbSe (20 mol% PbSe)	~2.85	7.14		4.50		54
	$GeSe_2$-As_2Se_3-PbSe (40 mol% PbSe)	~3.04	11.17		11.05		54,58–60
Form	Composition (mol%)	n_1 at λ = 1.55 µm	n_2 at λ = 1.55 µm ($\times 10^{-21}$ cm^2/W)		α_2 at λ = 1.55 µm (cm/GW)		Ref
Film	$Ge_{20}Te_{80}$	2.38	6.4				76
	$Ge_{20}Te_{78}Sb_2$	2.43	7.5				76
	$Ge_{20}Te_{76}Sb_4$	2.48	8.7				76
	$Ge_{20}Te_{70}Sb_{10}$	2.62	12.3				76
	$Ge_{23}Sb_7S_{70}$	2.17	3710		0.01		20
	$Ge_{23}Sb_7S_{70}$		9.3 (at 1.58 µm)				77
	Composition (mol%)	n_1 at λ = 4.515 µm	n_2 at λ = 4.515 µm		α_2 at λ = 4.515 µm		Ref
	$GeSe_2$-As_2Se_3-PbSe (40 mol% PbSe)	~3.14					56

Literature data on laser damage behavior of ChGs is important for broadband IR SC applications, though it is often limited, and does not always include details of measurement protocols, where pulsed, or single shot exposure performance differences, which can vastly impact the resulting material's behavior. Surface laser damage data as compared to bulk damage is often not distinguished, and lab-scale materials as compared to commercial glasses typically exhibit higher absorption characteristics or more surface defects due to limitations in optical fabrication capabilities. Hence, it is imperative when designing a material system for SC applications that this understanding of both processing and wavelength-specific properties and performance is noted. A short summary of pertinent laser damage data reported for ChGs is shown in Table 2, exhibiting quite clearly the typical reduction in damage resistance for bulk materials upon fiberization.

Table 2. A summary of laser damage values for a variety of ChG glasses in bulk and fiber forms. * indicates specifically surface damage resistance value and pulse duration of measurement.

Form	Composition (mol%)	Measurement λ (μm)	Laser Damage (MW/cm^2)	Ref
Bulk	$Ge_{28}Sb_{12}Se_{60}$	1.5	>1000	68
	$Ge_xAs_ySe_{1-x-y}$	1.064	1000–4000	69
	$Ge_{23}Sb_7S_{70}$	1.06	7200	27
	$Ge_{18}Ga_5Sb_7S_{70}$	1.06	6300	27
	$Ge_{18}Ga_5Sb_7S_{68}Se_2$	1.06	6000	27
	$Ge_{18}Ga_5Sb_7S_{65}Se_5$	1.06	5400	27
	$As_{24}S_{38}Se_{38}$	1.06	3500	27
	As_2S_3	1.06	8400 *	27
	$GeAs_2Se_2$	1.064	5500–6000	19
Fiber	As_2S_3	3.5	200	70
	As_2S_3	5.4	1000	71
	As_2S_3	1.5	1000	72
	As_2S_3	1.064	1800	73
	As-Se-Te	1.064	130	73
	As-Se-Te	2.94	30.6	73

As stated, there have been limited studies on optical properties of ChG glasses with planar geometries, especially candidate ChG glasses, which have been tailored for nonlinear photonic device applications at mid-infrared wavelengths and beyond. However, the planar, on-chip platform offers advantages such as integrating multi-signal processing functionalities onto a chip. Therefore, it is important to assess values measured from our GAP-Se film glasses with respect to a few reported values in literatures [20,67]. As a candidate glass for SC applications is (primarily) defined by its optical properties and damage resistance, its compatibility with the planned manufacturing method to final form (planar films or fiber) must be considered. Films made from simple binary glasses tend to be compatible with thermal evaporation methods, and some more complicated (ternary) glasses are amenable to solution derived processing methods either as glass [77] or organic/inorganic hybrids [79], with [80] or without [81] dopants. As noted for bulk materials above, variations in the deposition methods of thin films with identical composition can lead to concomitant variations in optical properties; thus, proper design of the processing method is also an important consideration for SC material fabrication [68]. Co-evaporation methods have been shown to be useful for the deposition of complex (>3) constituent glasses. However, deposition methodologies must be optimized and be compatible with both the processing method (avoiding preferential evaporation that leads to stoichiometric variation) and the underlying substrates (minimization of thermal expansion mismatch), as well as for their co-existence with other on-chip materials and their optical function.

Similar challenges exist for material selection of SC candidates for use in fiber form. A glass' viscosity (η)-temperature (T) behavior dictates an optimal draw temperature range as well as the materials' upper use temperature if the candidate SC material is to be used in fiber form. The

steepness of such a η-T curve for a given glass can vary dramatically across composition space, such as the As-Se system [see Figure 1a] that impacts (along with the glass' crystallization stability) the ease by which long lengths of low loss fiber can be processed [82,83]. Observe, for a small variation in As content (10–40 mol%), how the fiber draw temperature (typically shown to be in the 10^4–10^6 Pa·S range [83]) can vary by more than 100 K; additionally, note the subtle change in the d η/dT slope, which defines the temperature control needed over the possible drawing range (ΔT) that enables high quality fiber formation. Similarly, the composition and average bond strength of the glass' constituents defines the absolute position in temperature space for the η-T curve. As an example of the breadth of glass property variation, Figure 1b illustrates the variation of η-T curve for five commercially available SCHOTT glasses (IRG22–26) [84]. Shown are how each η-T curve (as measured via the probe penetration technique) varies with the network constituent (element) and their respective glass transition temperature, T_g, as both are defined by the glass' average bond strength. Hence, the definition of a glass with attractive optical properties may or may not have suitable manufacturability into fiber or film form.

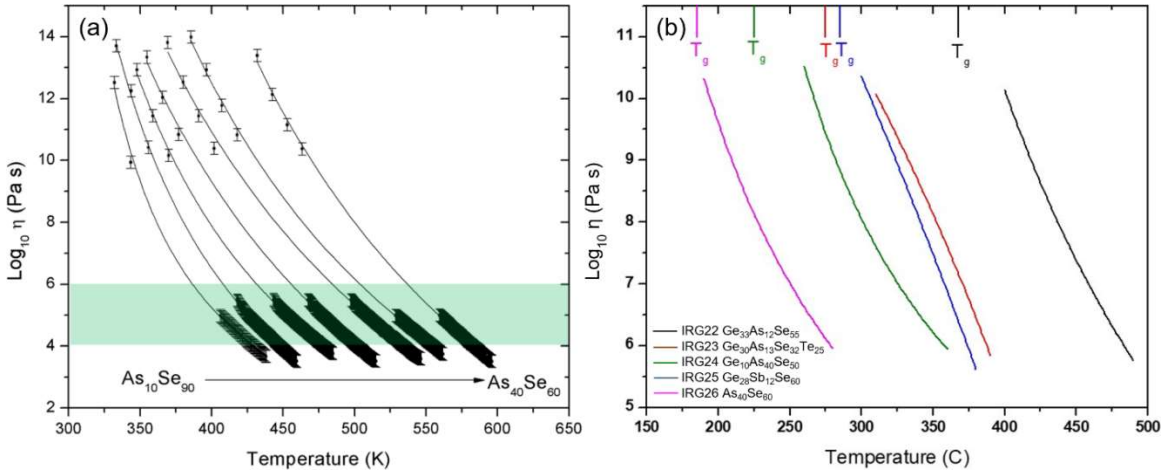

Figure 1. (**a**) Variation in η-T behavior as a function of composition within the binary As-Se system. The colored box is shown as a guide to the eye to illustrate the typical viscosity range for fiber drawing. Figure reproduced with permission from [83], © 2011 American Institute of Physics. (**b**) Viscosity data compilation (probe penetration method) for commercial reference materials over temperature range suitable for precision glass molding including relative position of glass transition temperature, T_g, as reported from the product data sheets. All curves are based on Sellmeir-paramaterization. (Curves for IRG23 and IRG25 show non-physical curvature over a broad temperature range and are only shown to illustrate the variation in temperature position and slope as a function of composition).

3. Composition, Morphology, and Optical Properties: Glasses Towards Glass Ceramics

Optical (nano)composites in the context of the present discussion are not homogeneous glasses; rather, they are multi-phase glass ceramics where a glass matrix contains embedded (nano)crystallites of desired refractive index, size, and size distribution throughout the composite's volume. The most commonly known optical composite is Zerodur [85], engineered for its transparency and superior (low) CTE. Zerodur is a lithia-alumino-silicate glass where nanocrystals with a small (~75 nm) size, narrow size distribution, and positive and negative CTE crystal phases are dispersed to realize the 'effective' physical property of interest, here, a near-zero CTE. The 'effective' aspect of the property of interest, CTE, can be approximated by the individual properties of the parent glass phase following the precipitation of the resulting crystal phases and the respective volume factions of each of the constituent phases (glass and crystallites). The refractive index mismatch between the crystal phase(s) and parent glass is small, leading to low loss in the spectral regime of interest. Similar efforts at making IR glass ceramics (composites) have been extensively studied by the researchers at the University of

Rennes [23,86–89] and others, as part of efforts to create low expansion substrates for optics suitable for use in applications in space as mirror substrates [25,90,91]. However, these composites were largely optimized for thermal and mechanical properties and not for their transmissive characteristics. There are few optical nanocomposites for use as transmissive bulk, film, or fiber components, such as those required for SC applications in the IR. This includes suitable MWIR and LWIR materials based on oxides or non-oxides. In this discussion, we do not consider tellurite glass materials, as they are not truly broadband. However, their high intensity performance as bulk and fiber may be attractive to SC application where MWIR performance is desired [92,93].

Exploitation of microstructural engineering in ChGs can enhance the thermal, mechanical, and optical properties for SC generation, and such tailoring presents vast opportunities for new optical function including as hosts for SC generation. In optical composites for SC generation, both the parent glass and the crystal phases impact the resulting linear/nonlinear optical, thermal, and mechanical properties; if composition, refractive index, crystallite type, size, and distribution are all carefully controlled and optimized, low loss transmissive components can be realized. Depending on the volume fraction and IR absorption characteristics of crystallites combined with their thermal (conductivity) characteristics, one could envision that laser damage behavior could also be enhanced by a secondary phase. Such thermal property engineering is being used with index matching strategies to create novel nanocrystal doped glasses for fiber laser applications [94–99]. As an example of composition, morphology, and eventual microstructure engineering possibilities for candidate SC material development, we discuss a model system based on a multi-component ChG system initially developed by the University of Rennes [23,86–89], where controlled nucleation and growth of secondary phase(s) were used to modify physical and optical properties. In the GAP-Se system where PbSe concentrations have been varied from 0 to 50 mol%, we have investigated base (homogeneous) glass as well as glasses following controlled nucleation and growth protocols to microstructurally vary physical and optical properties [54,59,63,65,66]. The optical performance of these GAP-Se glasses depends on the parent glass' morphology and post-heat treatment microstructure; specifically, each composition and fraction of co-existing phases. Based on examination of optical properties (bulk and film) evaluated to date, we explorde how such composite materials and the understanding of these factors could be further exploited to find desirable candidate materials for SC.

As a key first step to establish a process-structure-property relationship, Figure 2a shows the morphology phase diagram of GAP-Se glass with PbSe concentrations from 0 to 50 mol% [54,56,58,66], illustrating an immiscibility dome across a wide range of Pb concentrations from ~5–10 to ~45% at room temperature. Within these composition ranges, glasses melt-quenched from a temperature above a melting point to room temperature exhibit unstable liquid-liquid phase separation, yielding a homogeneous glass containing two amorphous phases. For lower PbSe content from 5–10 to 25–30 mol%, Pb-rich secondary phases have been shown to emerge within a Pb-deficient matrix while the morphology is inverted, becoming Pb-deficient secondary phases within a Pb-rich matrix as PbSe content increases beyond 25–30 up to 40–45 mol%. These regions are illustrated by two schematics in the diagram. Figure 2b,c show dark field (DF) transmission electron microscope (TEM) images collected from the glasses with 20 and 40 mol% of PbSe and linear profiles of atomic percentages for four constituents along the lines drawn in the DF TEM images. Specifically, the DF TEM image collected from the glass with 20 mol% PbSe includes bright, circular phases in a dark matrix, as shown in Figure 2b. The contrast in brightness between the secondary phases and the matrix in the DF TEM image suggests that the atomic percentage of heavy constituents in the secondary phases was greater than that in the matrix. The difference in weights of the secondary phase and the matrix is consistent with linear profiles where the atomic percentage of Pb, which is the heaviest constituent, was relatively high and low in the secondary phase and the matrix, respectively. In contrast, the DF TEM image and linear composition profiles collected from the glass with 20 mol% PbSe indicated an inverse microstructure with Pb-deficient secondary phases and a Pb-rich matrix, as shown in Figure 2c.

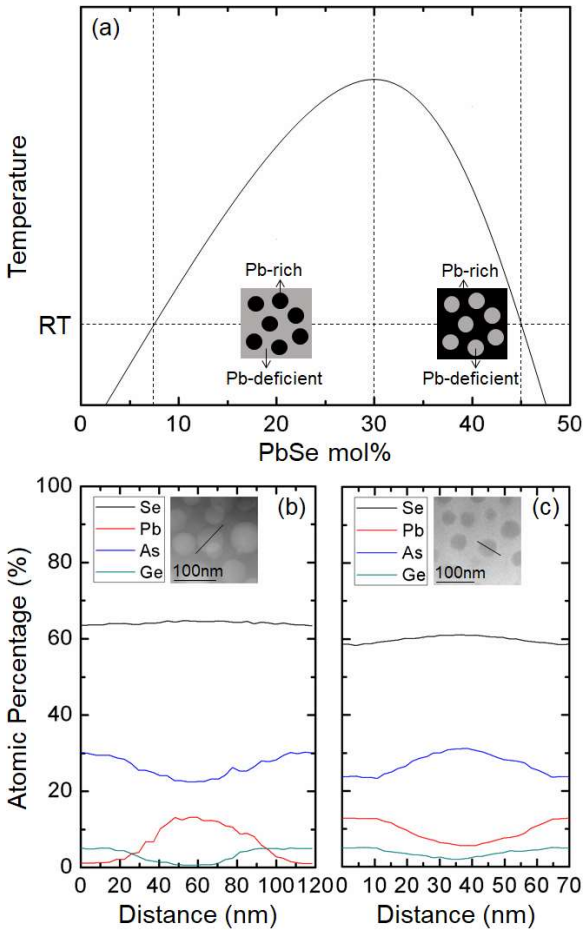

Figure 2. (**a**) An approximated phase diagram of $GeSe_2$-As_2Se_3-PbSe (GAP-Se) with an immiscibility dome illustrating two distinctly different inverse morphologies consisting of Pb-rich and Pb-deficient phases. (**b**,**c**) Linear profiles of atomic percentages for four constituents in glasses with 20 mol% and 40 mol% PbSe, respectively.

Here, we discuss the potential opportunity to extend the range of available SC materials that could be optimized for use through consideration of how, for example, two glass compositions within this composition space could be modified to form optical nanocomposites suitable for use in SC applications. Specifically, we consider these two glasses with 20 and 40 mol% PbSe, for two reasons: firstly, it is desirable that candidate materials have high linear and nonlinear refractive indices, which in general increase with the concentration of PbSe; here, such an increase must occur while maintaining the glass' transparency in the MWIR [58]. The refractive index-transparency criteria suggest that the concentration of PbSe needs to be high to increase linear and nonlinear refractive indices of the glasses, though below a certain point (~50–55 mol% PbSe), at which the entire volume of the material starts to become crystalline upon quenching, leading to optical losses [61,62]. Secondly, the phase-separated morphology observed within the immiscibility dome leads to a unique nucleation behavior of crystalline phases upon a heat treatment. Due to an energetically unstable state, Pb-rich phases can be transformed into crystals upon heat treatment while Pb-deficient phases remain amorphous [54,58,60,63–66]. These Pb-rich crystals have refractive indices far greater than those of their amorphous counterparts, making the effective linear and nonlinear refractive indices of glass-ceramic nanocomposites far greater than those of the parent glasses [56,59,60,66]. Furthermore, we have shown that the size of resulting crystalline phases typically range from 50 to 200 nm, making the nanocomposites effective media with respect to incident electromagnetic wave in the MWIR and LWIR. This enables the nanocomposite to maintain its transparency throughout the IR. In these prior studies, secondary phases have been induced by thermal and/or laser plus thermal heating.

How such material attributes would be impacted during film deposition or fiber drawing, for example, requires further consideration. Film studies in GAP-Se are ongoing for applications as gradient refractive index materials and other applications. To date, high quality (stoichiometric), low loss films of select GAP-Se glasses have been successfully made to thicknesses of 40 μm and have shown induced index and dispersion modification following crystallization as optical composites. Fiber drawing of GAP-Se has not, to date, been carried out. Here, additional scattering loss (due to crystal growth during reheat/fiberization) would need to be optimized so as to enhance optical properties, but not scatter loss. Such reheating of bulk preforms to make fiber would need to be optimized since the control of nucleation and growth near the fiber draw temperature could result in unwanted crystallization that leads to increase in loss.

4. Linear Optical Property Variation

The desirable linear optical properties of the glasses with specific compositions and corresponding microstructures are pre-requisites for a variety of optical applications. Figure 3a shows Fresnel loss corrected transmittance spectra for bulk GAP-Se glasses with 20 mol% and 40 mol% PbSe at wavelengths up to 10 μm. As can be seen, there is a clear difference in position of the glass' band edge, high energy tail states, and scatter can be observed, followed by near-100%, saturated transmittance at wavelengths from 2 to 10 μm. The spectral shift in band-edge energy is likely to be associated with the addition of highly-polarizing Pb elements where their interaction with other constituents in the glass creates additional energy bands within a bandgap which leads to a decrease in band-edge energy [65]. The tail near the band-edge originates from both band tail electronic states and light scattering which is highly dependent upon a combined effect from the size, volume fraction, and composition of secondary phases present in the phase separated glass. Here, the inverse secondary phase/matrix morphology and compositions of the glasses with 20 and 40 mol% PbSe give rise to such a difference, where the Pb-deficient phase dictates the edge position and the scattering is dictated by the refractive index contrast between the two phases [54,59]. The broad, high transparency window of these base glasses (no crystalline phase) across wavelengths from 2 to 10 μm strongly suggests that the material systems shown are effective media with low optical losses in both the MWIR and LWIR for SC applications. Figure 3b shows linear refractive indices and extinction coefficients of the planar disks of bulk glass with 20 and 40 mol% PbSe. The magnitude of refractive indices for both glasses was distinctively greater than those of other ChG glasses due to the existence of PbSe in the material matrix [65]. As the concentration of PbSe increases from 20 to 40 mol%, the refractive indices of the glasses correspondingly increased. A transition from a planar bulk disks to a film geometry (both with 40 mol% PbSe) resulted in a minor shift in band-edge energy and tail states, though it still maintains their maximum, near-100% intensity at wavelengths from 2 to 10 μm, as shown in Figure 3c. This is due to the fact that thin films of GAP-Se materials, regardless of composition, show no evidence of phase separation, and hence, reduced scatter loss. Meanwhile, Figure 3d shows that the refractive index of the film glass was greater than that of the planar bulk glass. This illustrates the impact of variation of thermal history and the more rapid cooling rate associated with film deposition and the resulting variation in bonding and density. As discussed earlier, the nature of materials with reduced geometries such as films was typically different from their bulk counterpart. This is due to a fact that source materials were condensed into an amorphous film with a relatively higher concentration of strained bonds on a room temperature or cold substrate, and therefore, vapor-deposited thin films were further from equilibrium compared to bulk counterparts [60].

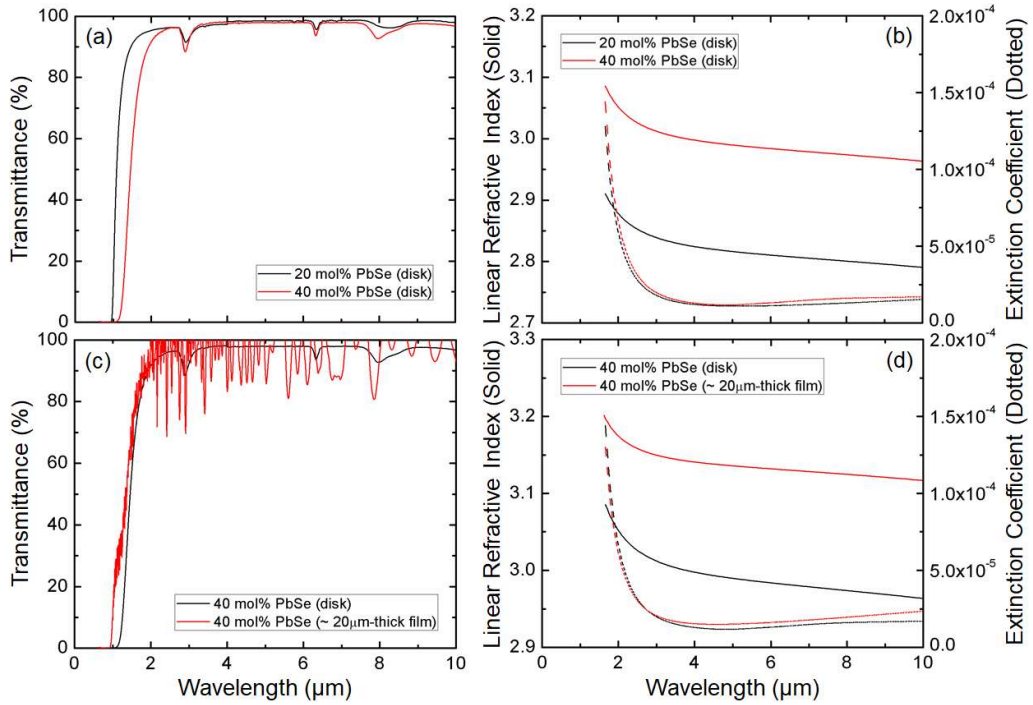

Figure 3. (**a**) Transmittance spectra of bulk GAP-Se glasses (t = 2 mm, polished disks) with 20 and 40 mol% PbSe. (**b**) Linear refractive indices (solid) and extinction coefficients (dashed) of bulk glasses with 20 mol% and 40 mol% PbSe measured by spectroscopic ellipsometry. (**c**) Transmittance spectra of bulk (t = 2 mm) and thin film (t ~20 μm) glasses with 40 mol% PbSe. (**d**) Linear refractive indices (solid) and extinction coefficients (dasged) of bulk and film glasses with 40 mol% PbSe measured by spectroscopic ellipsometry.

In studies to date, some properties of GAP-Se in bulk and film have been quantified across the broad spectral region where these materials operate. For optical designers, these attributes are critical to assessing and predicting optical performance. Using data presented in previous work and new to this work we summarized many of these optical property performance metrics for these glasses as a function of composition, form, and spectral region. Comparing the linear and nonlinear property variation (discussed in the next section) along with the dispersion variation of these glasses (see Table 3), one can see that both composition and form (bulk versus film) provides a 'knob' which allows a designer to modify their choice in material and form for desired application. Additionally, the promising nature of the base glass' FOM suggests further optimization through selected conversion to a glass ceramic, which may further enhance such properties.

Table 3. Key optical constants including Sellmeier coefficients, linear refractive index, Abbe number, and nonlinear figure of merit for bulk and film glasses with 20 and 40 mol% PbSe.

Composition & FormOptical Constant		20mol% PbSe	40mol% PbSe	
		Bulk	Bulk	Film
Sellmeir coefficient [90] $n=\sqrt{A+\frac{B\lambda^2}{\lambda^2-C^2}+\frac{D\lambda^2}{\lambda^2-E^2}}$		A = −20.6611 B = 28.5635 C = 0.2312 D = 10.4782 E = 90.4186	A = 4.1428 B = 4.7716 C = 0.5591 D = 41.6340 E = 168.4897	A = −17.9359 B = 27.7528 C = 0.1949 D = 1.4171 E = 36.6873
MWIR (4 μm–6 μm)	Linear refractive index	2.8387 at λ = 3 μm 2.8245 at λ = 4 μm 2.8164 at λ = 5 μm	3.0118 at λ = 3 μm 2.9977 at λ = 4 μm 2.9897 at λ = 5 μm	3.1495 at λ = 3 μm 3.1409 at λ = 4 μm 3.1358 at λ = 5 μm
	Abbe Number [91]	$\frac{n_{\lambda=4um}-1}{n_{\lambda=3um}-n_{\lambda=5\mu m}}=81.82$	$\frac{n_{\lambda=4um}-1}{n_{\lambda=3um}-n_{\lambda=5\mu m}}=90.39$	$\frac{n_{\lambda=4um}-1}{n_{\lambda=3um}-n_{\lambda=5um}}=156.27$
	Nonlinear refractive index	7.14×10^{-6} cm^2/GW at λ = 4 μm	11.17×10^{-6} cm^2/GW at λ = 4 μm	In progress
	Four-photon absorption coefficient	4.50×10^{-3} cm^5/GW^3 at λ = 4 μm	11.05×10^{-3} cm^5/GW^3 at λ = 4 μm	In progress
	Nonlinear figure of merit [92]	2.48×10^{-3} at λ = 4 μm	1.58×10^{-3} at λ = 4 μm	In progress
LWIR (8 μm–12 μm)	Linear refractive index	2.8007 at λ = 8 μm 2.7906 at λ = 10 μm 2.7793 at λ = 12 μm	2.9738 at λ = 8 μm 2.9634 at λ = 10 μm 2.9517 at λ = 12 μm	3.1248 at λ = 8 μm 3.1168 at λ = 10 μm 3.1071 at λ = 12 μm
	Abbe Number [91]	$\frac{n_{\lambda=10um}-1}{n_{\lambda=8um}-n_{\lambda=12um}}=83.67$	$\frac{n_{\lambda=10um}-1}{n_{\lambda=8um}-n_{\lambda=12um}}=88.84$	$\frac{n_{\lambda=10um}-1}{n_{\lambda=8um}-n_{\lambda=12um}}=119.59$

5. Nonlinear Optical Property Variation

In addition to high transparency and tailorable linear refractive index of the parent glass, the optical properties in a nonlinear regime are key attributes to SC materials, since self-phase modulation of incident light source scales with optical nonlinearity of a target material [3]. Figure 4a,b show Z-scan data for bulk glasses with 20 and 40 mol% PbSe, respectively. Each set of data includes two types of Z-scan measurements in closed and open modes where nonlinear refractive indices and multiphoton absorption coefficients are extracted from the closed and open modes, respectively. The Z-scan data in the closed mode are fitted with the following equation:

$$T_{CA}=1+\frac{4a\Delta\varphi_0\left(\frac{z}{z_0}\right)}{\left[1+\left(\frac{z}{z_0}\right)^2\right]\left[9+\left(\frac{z}{z_0}\right)^2\right]}$$

where T_{CA}, $\Delta\varphi_0$, z, and z_0 correspond to normalized transmittance in a closed-aperture mode, phase change of the laser beam due to nonlinear refraction, sample position, and Rayleigh length, respectively [78,100–103]. Values of $\Delta\varphi_0$ extracted from the fitting are inserted in the following equation to extract values of nonlinear refractive indices:

$$n_2=\frac{\Delta\varphi_0\lambda}{2\pi I_{00}L_{eff}}$$

where n_2, λ, I_{00}, and L_{eff} correspond to nonlinear refractive index, laser wavelength, peak intensity, and effective path length for multiphoton absorption, respectively [78,100–103]. The Z-scan data in the open mode are fitted with the following equation to extract multiphoton absorption coefficients:

$$T_{OA(nPA)}=\frac{1}{\{1+(n-1)\alpha_n L_{eff}[\frac{I_{00}}{(1+\left(\frac{z}{z_0}\right)^2}]^{n-1}\}^{\frac{1}{n-1}}}$$

where $T_{OA(nPA)}$, n, α_n correspond to normalized transmittance in an open-aperture mode, integer, and multiphoton absorption coefficient, respectively [78,100–103].

Figure 4c shows nonlinear refractive indices collected from four different locations of 20 and 40 mol% PbSe bulk glasses at 4.5 μm. The horizontal dotted lines, corresponding to average values, indicate that the nonlinear refractive index of the glasses increases from ~7.14 × 10^{-6} to ~1.17 × 10^{-6} cm^2/GW as the concentration of PbSe increases from 20 to 40 mol%. This corresponds to a change in the Pb-rich phase, changing from the secondary phase (in the 20% samples) to the matrix phase (40%) and a corresponding increase of absolute Pb content from (5.0 to 11.4 at%). While the magnitudes of the measured four-photon absorption coefficient are low for the glasses, the values likewise increase from ~4.50 × 10^{-3} to ~11.05 × 10^{-3} cm^5/GW^3 with increasing PbSe concentration, as shown in Figure 4d. Miller's rule dictates that an increase in optical linearity induces an increase in nonlinearity (n_2) and reduced optical band gap energy (E_g) [20]. The relationship is consistent with our experimental data where an increase in PbSe concentration from 20 to 40 mol% induces a red-shift of band-edge energy (dominated in part by scatter loss), an increase in linear refractive index, and an increase in nonlinear refractive index. These data are included for comparison in Table 3, along with a calculation of the two bulk glass' FOMs which are the same order of magnitude with that of Ge with high nonlinearity in MWIR [78]. As one can see, optical property tuning with the parent bulk glasses (prior to any further conversion to a glass ceramic) offers a variety of tailorable options for SC material design. Characterization of these same attributes in bulk glasses that have been partially converted to transparent optical nanocomposites are ongoing. Parallel studies to quantify other thermal and mechanical properties [55] in identical bulk glass samples are also in progress.

To assess how GAP-Se thin film glasses behave differently compared to their bulk counterpart in nonlinear regime, endeavors to explore and quantify the nonlinearity of films are expected to exhibit similar trends; however, we expect the magnitude of such changes and variation are likely different. These experiments, currently in progress, will help to define where further insight into the influence of material dimension on optical properties can be found. It is envisioned, as seen in planar base GAP-Se films, that similar tailoring of the resulting effective refractive index (while maintain low loss) and dispersion in a post-processed glass ceramic (dependent on volume fraction of phases formed) will enable effective nonlinear property modification as well. These enhancements, with a corresponding attention to the loss induced by a secondary phase will need to be evaluated, as a trade-off in assessing whether or not GAP-Se materials can be seriously considered as viable options for SC media.

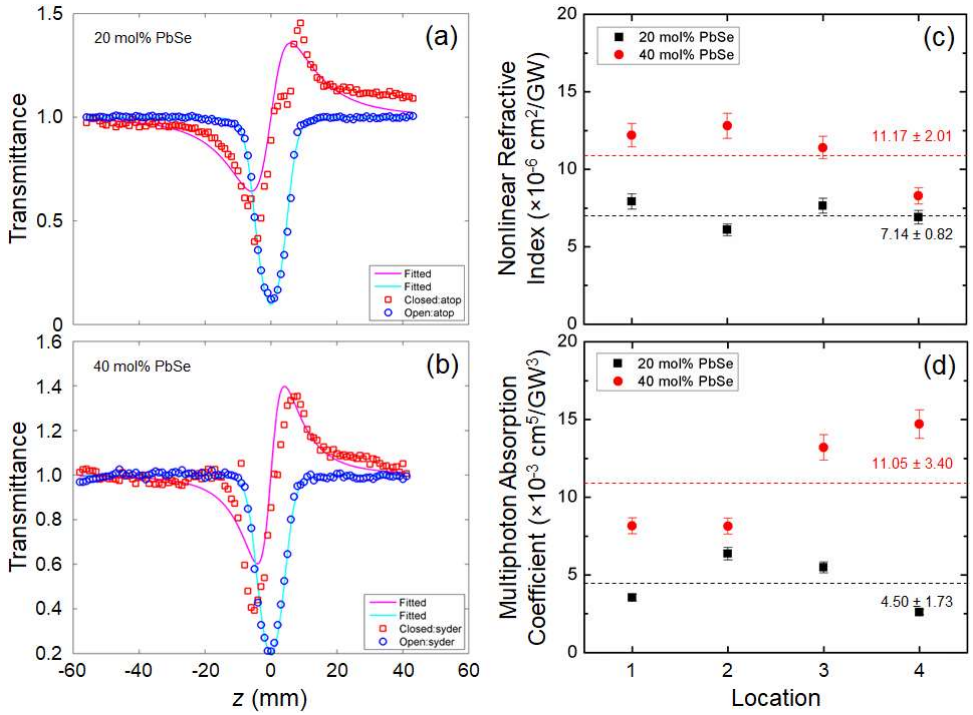

Figure 4. (**a**) Closed- and open-modes Z-scan profiles of a glass with 20 mol% PbSe (bulk coupons with t = 2 mm performed at a wavelength of 4.5 μm. (**b**) Closed- and open-mode Z-scan profiles of a glass with 40 mol% PbSe (bulk coupons with t = 2 mm). (**c**) Measured nonlinear refractive indices of glasses with 20 and 40 mol% PbSe at four different locations of the bulk samples. (**d**) Measured four-photon absorption coefficients for glasses with 20 and 40 mol% PbSe. The dashed lines represent the average of the measurements. The measurement error is estimated to be ~10%.

6. Conclusions

This paper reviews and summarizes the key optical and physical property attributes needed for materials being evaluated as candidates for SC generation. Following a summary of the key optical property criteria and those other physical properties which are impacted in the optical manufacturing of a component, we presented state-of-the art literature data for bulk glass, thin films, and fibers across the desired broadband spectral range of use. Employing a model broadband IR ChG system where extensive linear and initial nonlinear optical property data was collected, we have shown that novel multicomponent bulk GAP-Se ChG glasses exhibit high values of linear and nonlinear refractive indices which increase directly with Pb(Se) concentration, while maintaining high, broadband transparency, and low optical losses throughout the IR. Dispersion data has been calculated for bulk GAP-Se material and compared to thin films of the same composition, highlighting the variation of identical compositions and deposition-induced morphology variation (homogeneous films versus phase separated bulk glasses). The magnitudes of these optical parameters are found to be competitive with respect to those of commonly-used homogeneous ChG glasses in both linear and nonlinear optical regimes, as quantified by their nonlinear FOM. Further efforts to extend our understanding of this system, both as bulk glasses and in thin film or fiber form, will allow us to assess the glass' viability as potential SC hosts.

Supplementary Materials: Supplementary materials can be found at http://www.mdpi.com/2076-3417/8/11/2082/s1.

Author Contributions: K.R., C.G. and M.K. conceived and designed the study. C.G. fabricated bulk specimens. G.Y. and J.H. fabricated thin film specimens. M.K. performed linear optical characterization and microstructure analysis. B.-U.S. and D.T.H.T. conducted nonlinear optical characterization. All authors wrote the manuscript together. K.R. supervised the project.

Acknowledgments: C.G. and M.K. acknowledge the partial support of UCF's Pre-eminent Post-doctoral Scholar Program (P3). G.Y. and J.H. were supported in part by National Science Foundation under award #1506605. B.-U.S. and D.T.H.T. acknowledge the support of the MOE ACRF Tier 2 grant and National Research Foundation Competitive Research Program Grant. The authors thank A. V. Pogrebnyakov for spectroscopic ellipsometry characterization.

Conflicts of Interest: The authors declare no conflict of interest.

References

1. Du, Q.; Luo, Z.; Zhong, H.; Zhang, Y.; Huang, Y.; Du, T.; Zhang, W.; Gu, T.; Hu, J. Chip-scale broadband spectroscopic chemical sensing using an integrated supercontinuum source in a chalcogenide glass waveguide. *Photon. Res.* **2018**, *6*, 506–510. [CrossRef]
2. Eggleton, B.; Luther-Davies, B.; Richardson, K. Chalcogenide photonics. *Nat. Photonics* **2011**, *5*, 141. [CrossRef]
3. Mandon, J.; Sorokin, E.; Sorokina, I.; Guelachvili, G.; Picqué, N. Supercontinua for high-resolution absorption multiplex infrared spectroscopy. *Opt. Lett.* **2008**, *33*, 285–287. [CrossRef]
4. Wang, T.; Ng, D.; Ng, S.; Toh, Y.; Chee, A.; Chen, G.; Wang, Q.; Tan, D. Supercontinuum generation in bandgap engineered, back-end CMOS compatible silicon rich nitride waveguides. *Laser Photonics Rev.* **2015**, *9*, 498–506. [CrossRef]
5. Johnson, A.; Mayer, A.; Klenner, A.; Luke, K.; Lamb, E.; Lamont, M.; Joshi, C.; Okawachi, Y.; Wise, F.; Lipson, M.; et al. Octave-spanning coherent supercontinuum generation in a silicon nitride waveguide. *Opt. Lett.* **2015**, *40*, 5117–5120. [CrossRef]
6. Hsieh, I.; Chen, X.; Liu, X.; Dadap, J.; Panoiu, N.; Chou, C.; Xia, F.; Green, W.; Vlasov, Y.; Osgood, R. Supercontinuum generation in silicon photonic wires. *Opt. Express* **2007**, *15*, 15242–15249. [CrossRef]
7. Chen, L.; Chen, F.; Dai, S.; Tao, G.; Yan, L.; Shen, X.; Ma, H.; Zhang, X.; Xu, Y. Third-order nonlinearity in Ge–Sb–Se glasses at mid-infrared wavelengths. *Mater. Res. Bull.* **2015**, *70*, 204–208. [CrossRef]
8. Zakery, A.; Elliott, S. Optical properties and applications of chalcogenide glasses: A review. *J. Non-Cryst. Solids* **2003**, *330*, 1–2. [CrossRef]
9. Anashkina, E.; Shiryaev, V.; Snopatin, G.; Muraviev, S.; Kim, A. On the possibility of mid-IR supercontinuum generation in As-Se-Te/As-S core/clad fibers with all-fiber femtosecond pump source. *J. Non-Cryst. Solids* **2018**, *480*, 38–42. [CrossRef]
10. Patrick, H.; Frédéric, S.; Vincent, C.; Johann, T.; Ludovic, G. Selenide glass single mode optical fiber for nonlinear optics. *Opt. Mater.* **2007**, *29*, 651–656. [CrossRef]
11. Monro, T.; Ebendorff-Heidepriem, H. Progress in Microstructured Optical Fibers. *Annu. Rev. Mater. Res.* **2006**, *36*, 467–495. [CrossRef]
12. Savelli, I.; Mouawad, O.; Fatome, J.; Kibler, B.; Désévédavy, F.; Gadret, G.; Jules, J.; Bony, P.; Kawashima, H.; Gao, W.; et al. Mid-infrared 2000-nm bandwidth supercontinuum generation in suspended-core microstructured Sulfide and Tellurite optical fibers. *Opt. Express* **2012**, *20*, 27083–27093. [CrossRef]
13. Kohoutek, T.; Yan, X.; Shiosaka, T.; Yannopoulos, S.; Chrissanthopoulos, A.; Suzuki, T.; Ohishi, Y. Enhanced Raman gain of Ge-Ga-Sb-S chalcogenide glass for highly nonlinear microstructured optical fibers. *JOSA B* **2011**, *28*, 2284–2290. [CrossRef]
14. Dantanarayana, H.; Abdel-Moneim, N.; Tang, Z.; Sojka, L.; Sujecki, S.; Furniss, D.; Seddon, A.; Kubat, I.; Bang, O.; Benson, T. Refractive index dispersion of chalcogenide glasses for ultra-high numerical-aperture fiber for mid-infrared supercontinuum generation. *Opt. Mater. Express* **2014**, *4*, 1444–1455. [CrossRef]
15. Petersen, C.; Møller, U.; Kubat, I.; Zhou, B.; Dupont, S.; Ramsay, J.; Benson, T.; Sujecki, S.; Abdel-Moneim, N.; Tang, Z.; et al. Mid-infrared supercontinuum covering the 1.4–13.3 µm molecular fingerprint region using ultra-high NA chalcogenide step-index fibre. *Nat. Photonics* **2014**, *8*, 830. [CrossRef]
16. Boudebs, G.; Cherukulappurath, S.; Leblond, H.; Troles, J.; Smektala, F.; Sanchez, F. Experimental and theoretical study of higher-order nonlinearities in chalcogenide glasses. *Opt. Commun.* **2003**, *219*, 427–433. [CrossRef]
17. Gao, W.; Liao, M.; Yan, X.; Kito, C.; Kohoutek, T.; Suzuki, T.; El-Amraoui, M.; Jules, J.; Gadret, G.; Desevedavy, F.; et al. Visible Light Generation and Its Influence on Supercontinuum in Chalcogenide As_2S_3 Microstructured Optical Fiber. *Appl. Phys. Express* **2011**, *4*, 102601. [CrossRef]

18. El-Amraoui, M.; Fatome, J.; Jules, J.; Kibler, B.; Gadret, G.; Fortier, C.; Smektala, F.; Skripatchev, I.; Polacchini, C.; Messaddeq, Y.; et al. Strong infrared spectral broadening in low-loss As-S chalcogenide suspended core microstructured optical fibers. *Opt. Express* **2010**, *18*, 4547–4556. [CrossRef]
19. Troles, J.; Smektala, F.; Boudebs, G.; Monteil, A.; Bureau, B.; Lucas, J. Chalcogenide glasses as solid state optical limiters at 1.064 μm. *Opt. Mater.* **2004**, *25*, 231–237. [CrossRef]
20. Choi, J.; Han, Z.; Sohn, B.; Chen, G.; Smith, C.; Kimerling, L.; Richardson, K.; Agarwal, A.; Tan, D. Nonlinear characterization of GeSbS chalcogenide glass waveguides. *Sci. Rep.* **2016**, *6*, 39234. [CrossRef]
21. Olivier, M.; Tchahame, J.; Němec, P.; Chauvet, M.; Besse, V.; Cassagne, C.; Boudebs, G.; Renversez, G.; Boidin, R.; Baudet, E.; et al. Structure, nonlinear properties, and photosensitivity of $(GeSe_2)_{100-x}(Sb_2Se_3)_x$ glasses. *Opt. Mater. Express* **2014**, *4*, 525–540. [CrossRef]
22. Liu, Q.; Zhao, X.; Tanaka, K.; Narazaki, A.; Hirao, K.; Gan, F. Second-harmonic generation in Ge-As-S glasses by electron beam irradiation and analysis of the poling mechanism. *Opt. Commun.* **2001**, *198*, 187–192. [CrossRef]
23. Rozé, M.; Calvez, L.; Ledemi, Y.; Allix, M.; Matzen, G.; Zhang, X. Optical and Mechanical Properties of Glasses and Glass–Ceramics Based on the Ge-Ga-Se System. *J. Am. Ceram. Soc.* **2008**, *91*, 3566–3570. [CrossRef]
24. Zhang, X.; Bureau, B.; Lucas, P.; Boussard-Pledel, C.; Lucas, J. Glasses for Seeing Beyond Visible. *Chem. Eur. J.* **2008**, *14*, 432–442. [CrossRef] [PubMed]
25. Vigreux-Bercovici, C.; Ranieri, V.; Labadie, L.; Broquin, J.; Kern, P.; Pradel, A. Waveguides based on $Te_2As_3Se_5$ thick films for spatial interferometry. *J. Non-Cryst. Solids* **2006**, *352*, 2416–2419. [CrossRef]
26. Wang, T.; Gai, X.; Wei, W.; Wang, R.; Yang, Z.; Shen, X.; Madden, S.; Luther-Davies, B. Systematic z-scan measurements of the third order nonlinearity of chalcogenide glasses. *Opt. Mater. Express.* **2014**, *4*, 1011–1022. [CrossRef]
27. Stegeman, R.; Stegeman, G.; Delfyett, P., Jr.; Petit, L.; Carlie, N.; Richardson, K.; Couzi, M. Raman gain measurements and photo-induced transmission effects of germanium- and arsenic-based chalcogenide glasses. *Opt. Express.* **2006**, *14*, 11702–11708. [CrossRef] [PubMed]
28. Cerqua-Richardson, K.; McKinley, J.; Lawrence, B.; Joshi, S.; Villeneuve, A. Comparison of nonlinear optical properties of sulfide glasses in bulk and thin film form. *Opt. Mater.* **1998**, *10*, 155–159. [CrossRef]
29. Serna, S.; Lin, H.; Alonso-Ramos, C.; Yadav, A.; Le Roux, X.; Richardson, K.; Cassan, E.; Dubreuil, N.; Hu, J.; Vivien, L. Nonlinear optical properties of integrated GeSbS chalcogenide waveguides. *Photonics Res.* **2018**, *6*, B37–B42. [CrossRef]
30. Zou, L.E.; He, P.P.; Chen, B.X.; Iso, M. Nonlinear optical properties of $As_{20}S_{80}$ system chalcogenide glass using Z-scan and its strip waveguide under bandgap light using the self-phase modulation. *AIP Adv.* **2017**, *7*, 025003. [CrossRef]
31. Almeida, J.M.P.; Barbano, E.C.; Arnold, C.B.; Misoguti, L.; Mendonca, C.R. Nonlinear optical waveguides in As_2S_3-Ag_2S chalcogenide glass thin films. *Opt. Mater. Express* **2017**, *7*, 93–99. [CrossRef]
32. Krogstad, M.R.; Ahn, S.; Park, W.; Gopinath, J. Nonlinear characterization of $Ge_{28}Sb_{12}Se_{60}$ bulk and waveguide devices. *Opt. Express* **2015**, *6*, 7870–7878. [CrossRef]
33. Yu, Y.; Gai, X.; Ma, P.; Choi, D.-Y.; Yang, Z.; Wang, R.; Debbarma, S.; Madden, S.J.; Luther-Davies, B. A broadband, quasi-continuous, mid-infrared supercontinuum generated in a chalcogenide glass waveguide. *Laser Photonics Rev.* **2014**, *8*, 792–798. [CrossRef]
34. Yu, Y.; Gai, X.; Ma, P.; Vu, K.; Yang, Z.; Wang, R.; Choi, D.-Y.; Madden, S.; Luther-Davies, B. Experimental demonstration of linearly polarized 2–10 μm supercontinuum generation in a chalcogenide rib waveguide. *Opt. Lett.* **2016**, *41*, 958–961. [CrossRef]
35. Tremblay, J.-E.; Malinowski, M.; Richardson, K.; Fathpour, S.; Wu, M.C. Picojoule-level octave-spanning supercontinuum generation in chalcogenide waveguides. *Opt. Express* **2018**, *26*, 21358–21363. [CrossRef]
36. Miyashita, T.; Terunuma, Y. Optical transmission loss of As–S fiber in 1.0–55μm wavelength region. *Jpn. J. Appl. Phys.* **1982**, *21*, 75. [CrossRef]
37. Hattori, H.; Sato, S.; Fujioka, T. High power CO laser transmission through As–S glass fibers. *Electron. Lett.* **1984**, *20*, 811–812. [CrossRef]
38. Gattass, R.R.; Shaw, L.B.; Nguyen, V.Q.; Pureza, P.C.; Aggarwal, I.D.; Sanghera, J.S. All-fiber chalcogenide-based mid-infrared supercontinuum source. *Opt. Fiber Technol.* **2012**, *18*, 345–348. [CrossRef]

39. Marandi, A.; Rudy, C.W.; Plotnichenko, V.G.; Dianov, E.M.; Vodopyanov, K.L.; Byer, R.L. Mid-infrared supercontinuum generation in tapered chalcogenide fiber for producing octave-spanning frequency comb around 3 µm. *Opt. Express* **2012**, *20*, 24218–24225. [CrossRef]
40. Deng, D.; Liu, L.; Tuan, T.H.; Kanou, Y.; Matsumoto, M.; Tezuka, H.; Suzuki, T.; Ohishi, Y. Mid-infrared supercontinuum covering 3–10 µm using a As_2Se_3 core and As_2S_5 cladding step-index chalcogenide fiber. *J. Ceram. Soc. Jpn.* **2016**, *124*, 103–105. [CrossRef]
41. Kedenburg, S.; Steinle, T.; Mörz, F.; Steinmann, A.; Giessen, H. High-power mid-infrared high repetition-rate supercontinuum source based on a chalcogenide step-index fiber. *Opt. Lett.* **2015**, *40*, 2668–2671. [CrossRef] [PubMed]
42. Møller, U.; Yu, Y.; Kubat, I.; Petersen, C.R.; Gai, X.; Brilland, L.; Méchin, D.; Caillaud, C.; Troles, J.; Luther-Davies, B.; Bang, O. Multi-milliwatt mid-infrared supercontinuum generation in a suspended core chalcogenide fiber. *Opt. Express* **2015**, *23*, 3282–3291. [CrossRef] [PubMed]
43. Cheng, T.; Nagasaka, K.; Tuan, T.H.; Xue, X.; Matsumoto, M.; Tezuka, H.; Suzuki, T.; Ohishi, Y. Mid-infrared supercontinuum generation spanning 2.0 to 15.1 µm in a chalcogenide step-index fiber. *Opt. Lett.* **2016**, *41*, 2117–2120. [CrossRef] [PubMed]
44. Zhang, B.; Yu, Y.; Zhai, C.; Qi, S.; Wang, Y.; Yang, A.; Gai, X.; Wang, R.; Yang, Z.; Luther-Davies, B. High brightness 2.2–12 µm mid-infrared supercontinuum generation in a nontoxic chalcogenide step-index fiber. *J. Am. Ceramic Soc.* **2016**, *99*, 2565–2568. [CrossRef]
45. Yu, Y.; Zhang, B.; Gai, X.; Zhai, C.; Qi, S.; Guo, W.; Yang, Z.; Wang, R.; Choi, D.-Y.; Madden, S.; et al. 1.8–10 µm mid-infrared supercontinuum generated in a step-index chalcogenide fiber using low peak pump power. *Opt. Lett.* **2015**, *40*, 1081–1084. [CrossRef] [PubMed]
46. Karim, M.R.; Rahman, B.M.A.; Agrawal, G.P. Mid-infrared supercontinuum generation using dispersion-engineered $Ge_{11.5}As_{24}Se_{64.5}$ chalcogenide channel waveguide. *Opt. Express* **2015**, *23*, 6903–6914. [CrossRef] [PubMed]
47. Yeom, D.-I.; Mägi, E.C.; Lamont, M.R.E.; Roelens, M.A.F.; Fu, L.; Eggleton, B.J. Low-threshold supercontinuum generation in highly nonlinear chalcogenide nanowires. *Opt. Lett.* **2008**, *33*, 660–662. [CrossRef] [PubMed]
48. Psaila, N.D.; Thomson, R.R.; Bookey, H.T.; Shen, S.X.; Chiodo, N.; Osellame, R.; Cerullo, G.; Jha, A.; Kar, A.K. Supercontinuum generation in an ultrafast laser inscribed chalcogenide glass waveguide. *Opt. Express* **2007**, *15*, 15776–15781. [CrossRef]
49. Lamont, M.R.E.; Luther-Davies, B.; Choi, D.-Y.; Madden, S.; Eggleton, B.J. Supercontinuum generation in dispersion engineered highly nonlinear (γ = 10 /W/m) As_2S_3 chalcogenide planar waveguide. *Opt. Express* **2008**, *16*, 14938–14944. [CrossRef] [PubMed]
50. Gai, X.; Choi, D.-Y.; Madden, S.; Yang, Z.; Wang, R.; Luther-Davies, B. Supercontinuum generation in the mid-infrared from a dispersion-engineered As_2S_3 glass rib waveguide. *Opt. Lett.* **2012**, *37*, 3870–3872. [CrossRef] [PubMed]
51. Cherukulappurath, S.; Guignard, M.; Marchand, C.; Smektala, F.; Boudebs, G. Linear and nonlinear optical characterization of tellurium based chalcogenide glasses. *Opt. Commun.* **2004**, *242*, 313–319. [CrossRef]
52. Belykh, A.V.; Efimov, O.M.; Glebov, L.B.; Matveev, Y.A.; Mekryukov, A.M.; Mikhailov, M.D.; Richardson, K.A. Photo-structural Transformation of Chalcogenide glasses under Nonlinear Absorption of Laser Radiation. *J. Non-Cryst. Solids* **1997**, *213*, 330–335. [CrossRef]
53. Tanaka, K. Photoinduced Deformation in Chalcogenide Glasses. In *Amorphous Chalcogenides, Advances and Applications*; Wang, R., Ed.; Pan Stanford Publishing: Boca Raton, FL, USA, 2014.
54. Buff, A. A Study of Crystallization Behavior in Phase Separated Chalcogenide Glasses. Ph.D. Thesis, University of Central Florida, Orlando, FL, USA, 2016.
55. Fauvel, V. Synthesis and Mechanical Properties of Chalcogenide Glass-Ceramics. Master's Thesis, ENSIL-ENSCI Ecole d'Ingénieurs de Limoges, Limoges, France, 2018.
56. Kang, M.; Swisher, A.M.; Pogrebnyakov, A.V.; Liu, L.; Kirk, A.; Aiken, S.; Sisken, L.; Lonergan, C.; Cook, J.; Malendevych, T.; et al. Ultra-Low Dispersion Multicomponent Thin Film Chalcogenide Glass for Broadband Gradient Index Optics. *Adv. Mater.* **2018**, *30*, 1803628. [CrossRef] [PubMed]
57. Yadav, A.; Kang, M.; Goncalves, C.; Sisken, L.; Blanco, C.; Arias, C.; Riveiro-Baleine, C.; Richardson, K. Index and Dispersion engineering of GeSe2-As2Se3-PbSe chalcogenide glasses through purification. **2018**, submitted.

58. Kang, M.; Sisken, L.; Cook, J.; Blanco, C.; Richardson, M.; Mingareev, I.; Richardson, K. Refractive Index Patterning of Infrared Glass Ceramics through Laser-Induced Vitrification. *Opt. Mater. Express* **2018**, *8*, 2722–2733. [CrossRef]
59. Sisken, L. Laser-Induced Crystallization Mechanisms in Chalcogenide Glass Materials for Advanced Optical Functionality. Ph.D. Thesis, University of Central Florida, Orlando, FL, USA, 2017.
60. Sisken, L.; Smith, C.; Buff, A.; Kang, M.; Chamma, K.; Wachtel, P.; Musgraves, J.; Rivero-Baleine, C.; Kirk, A.; Kalinowski, M.; et al. Evidence of spatially selective refractive index modification in 15$GeSe_2$-45As_2Se_3-40PbSe glass through correlation of structure and optical property measurements for GRIN applications. *Opt. Mater. Express* **2017**, *7*, 3077–3092. [CrossRef]
61. Yang, G.; Zhang, X.; Ren, J.; Yunxia, Y.; Chen, G.; Ma, H.; Adam, J. Glass formation and properties of chalcogenide in a $GeSe_2$-As_2Se_3-PbSe system. *J. Am. Ceram. Soc.* **2007**, *90*, 1500–1503. [CrossRef]
62. Wang, H.; Zhang, X.; Yang, G.; Xu, Y.; Ma, H.; Adam, J.; Gu, Z.; Chen, G. Micro-crystallization of the infrared transmitting chalcogenide glass in $GeSe_2$-As_2Se_3-PbSe system. *Ceram. Int.* **2009**, *35*, 83–86. [CrossRef]
63. Richardson, K.; Kang, M.; Sisken, L.; Yadav, A.; Blanco, C.; Antia, M.; Novak, S.; Gleason, B.; Smith, C.; Buff, A.; et al. Advances in infrared GRIN: A review of novel materials towards components and devices. *Proc. SPIE* **2018**, *10627*, 106270A.
64. Richardson, K.; Buff, A.; Smith, C.; Sisken, L.; Musgraves, J.; Wachtel, P.; Mayer, T.; Swisher, A.; Pogrebnyakov, A.; Kang, M.; et al. Engineering novel infrared glass ceramics for advanced optical solutions. *Proc. SPIE* **2016**, *9822*, 982205.
65. Yadav, A.; Kang, M.; Smith, C.; Lonergan, J.; Buff, A.; Sisken, L.; Chamma, K.; Blanco, C.; Caraccio, J.; Mayer, T.; et al. Influence of phase-separation on structure-property relationships in the $(GeSe_2$-$3As_2Se_3)_{1-x}PbSe_x$ glass system. *Phys. Chem. Glasses-B* **2017**, *58*, 115–126. [CrossRef]
66. Yadav, A.; Buff, A.; Kang, M.; Sisken, L.; Smith, C.; Lonergan, J.; Blanco, C.; Antia, M.; Driggers, M.; Kirk, A.; et al. Melt property variation in $GeSe_2$-As_2Se_3-PbSe glass ceramics for infrared gradient refractive index (GRIN) applications. *Int. J. Appl. Glass Sci.* **2018**. [CrossRef]
67. Hu, J.; Feng, N.; Carlie, N.; Petit, L.; Wang, J.; Agarwal, A.; Richardson, K.; Kimerling, L. Demonstration of Low-Loss High-Index-Contrast Planar Glass Waveguides with Graded-Index Cladding Layers. *Opt. Express* **2007**, *15*, 14566–14572. [CrossRef] [PubMed]
68. Lenz, G.; Zimmermann, J.; Katsufuji, T.; Lines, M.E.; Hwang, H.Y.; Spalter, S.; Slusher, R.E.; Cheong, S.-W.; Sanghera, J.S.; Aggarwal, I.D. Large Kerr effect in bulk Se-based chalcogenide glasses. *Opt. Lett.* **2000**, *25*, 254–256. [CrossRef] [PubMed]
69. Prasad, A.; Zha, C.-J.; Wang, R.-P.; Smith, A.; Madden, S.; Luther-Davies, B. Properties of $Ge_xAs_ySe_{1-x-y}$ glasses for all-optical signal processing. *Opt. Express* **2008**, *16*, 2804–2815. [CrossRef] [PubMed]
70. Busse, L.E.; Moon, J.A.; Sanghera, J.S.; Aggarwal, I.D. Chalcogenide fibers deliver high IR power. *Laser Focus World* **1996**, *32*, 143–150.
71. Aggarwal, I.D.; Sanghera, J.S. Development and applications of chalcogenide glass optical fibers at NRL. *J. Optoelectron. Adv. Mater.* **2002**, *4*, 665–678.
72. Kulkarni, O.P.; Xia, C.; Lee, D.J.; Kumar, M.; Kuditcher, A.; Islam, M.N.; Terry, F.L.; Freeman, M.J., Jr.; Aitken, B.G.; Currie, S.; et al. Third order cascaded Raman wavelength shifting in chalcogenide fibers and determination of Raman gain coefficient. *Opt. Express* **2006**, *14*, 7924–7930. [CrossRef] [PubMed]
73. Papagiakoumou, E.; Papadopoulos, D.N.; Serafetinides, A.A. Pulsed infrared radiation transmission through chalcogenide glass fibers. *Opt. Commun.* **2007**, *276*, 80–86. [CrossRef]
74. Boudebs, G.; Sanchez, F.; Troles, J.; Smektala, F. Nonlinear optical properties of chalcogenide glasses: Comparison between Mach–Zehnder interferometry and Z-scan techniques. *Opt. Commun.* **2001**, *199*, 425–433. [CrossRef]
75. Quémard, C.; Smektala, F.; Couderc, V.; Barthélémy, A.; Lucas, J. Chalcogenide glasses with high non linear optical properties for telecommunications. *J. Phys. Chem. Solids* **2001**, *62*, 1435–1440. [CrossRef]
76. Kumar, P.; Kaur, J.; Tripathi, S.; Sharma, I. Effect of antimony (Sb) addition on the linear and non-linear optical properties of amorphous Ge-Te-Sb thin films. *Indian J. Phys.* **2017**, *91*, 1503–1511. [CrossRef]
77. Waldmann, M.; Musgraves, J.D.; Richardson, K.; Arnold, C.B. Structural properties of solution processed $Ge_{23}Sb_7S_{70}$ glass materials. *J. Mater. Chem.* **2012**, *22*, 17848–17852. [CrossRef]
78. Sohn, B.-U.; Monmeyran, C.; Kimerling, L.C.; Agarwal, A.M.; Tan, D.T.H. Kerr nonlinearity and multi-photon absorption in germanium at mid-infrared wavelengths. *Appl. Phys. Lett.* **2017**, *111*, 091902. [CrossRef]

79. Zou, Y.; Moreel, L.; Lin, H.; Zhou, J.; Li, L.; Danto, S.; Musgraves, J.D.; Richardson, K.; Dobson, K.D.; Birkmire, R.; et al. Solution Processing and Resist-Free Nanoimprint Fabrication of Thin Film Chalcogenide Glass Devices: Inorganic-Organic Hybrid Photonic Integration. *Adv. Opt. Mater.* **2014**, *2*, 759–764. [CrossRef]
80. Li, C.; Novak, S.; Richardson, K.; Deng, W. Electrospray deposition of quantum dot-doped $Ge_{23}Sb_7S_{70}$ chalcogenide glass films. *Thin Solid Films* **2017**, *624*, 194–199. [CrossRef]
81. Novak, S.; Li, C.; Borodinov, N.; Han, Z.; Monmeyran, C.; Patel, N.; Du, Q.; Lumdee, C.; Kik, P.; Deng, W.; et al. Electrospray deposition of uniform thickness $Ge_{23}Sb_7S_{70}$ and $As_{40}S_{60}$ chalcogenide glass films. *J. Vis. Exp.* **2016**. [CrossRef] [PubMed]
82. Yang, G.; Rouxel, T.; Troles, J.; Bureau, B.; Boussard-Plédel, C.; Houizot, P.; Sangleboeuf, J.-C. Viscosity of As_2Se_3 glass during the fiber drawing process. *J. Am. Ceram. Soc.* **2011**, *94*, 2408–2411. [CrossRef]
83. Musgraves, J.; Wachtel, P.; Novak, S.; Wilkinson, J.; Richardson, K. Composition dependence of the viscosity and other physical properties in the arsenic selenide glass system. *J. Appl. Phys.* **2011**, *110*, 063503. [CrossRef]
84. Schott Advanced Optics. Available online: https://www.schott.com/advanced_optics/english/products/optical-materials/ir-materials/infrared-chalcogenide-glasses/index.html (accessed on 1 September 2018).
85. Schott Zerodur. Available online: https://www.schott.com/d/advanced_optics/e532f55f-d6c1-4748-8c60-886eaca1daf5/1.2/schott-zerodur-general-may-2013-eng.pdf (accessed on 1 September 2018).
86. Lin, C.; Calvez, L.; Ying, L.; Chen, F.; Song, B.; Shen, X.; Dai, S.; Zhang, X. External influence on third-order optical nonlinearity of transparent chalcogenide glass-ceramics. *Appl. Phys. A* **2011**, *104*, 615–620. [CrossRef]
87. Hubert, M.; Delaizir, G.; Monnier, J.; Godart, C.; Ma, H.; Zhang, X.; Calvez, L. An innovative approach to develop highly performant chalcogenide glasses and glass-ceramics transparent in the infrared range. *Opt. Express* **2011**, *19*, 23513–23522. [CrossRef] [PubMed]
88. Calvez, L.; Ma, H.; Lucas, J.; Zhang, X. Preparation and properties of glasses and glass-ceramics based on $GeSe_2$-Sb_2Se_3 and halides. *Phys. Chem. Glasses Eur. J. Glass Sci. Technol. Part B* **2006**, *47*, 142–145.
89. Calvez, L.; Ma, H.; Lucas, J.; Zhang, X. Selenium-Based Glasses and Glass Ceramics Transmitting Light from the Visible to the Far-IR. *Adv. Mater.* **2007**, *19*, 129–132. [CrossRef]
90. Ghosh, G. Sellmeir coefficients and dispersion of thermo-optic coefficients for some optical glasses. *Appl. Opt.* **1997**, *36*, 1540–1546. [CrossRef] [PubMed]
91. Gibson, D.; Bayya, S.; Nguyen, V.; Sanghera, J.; Kotov, M.; Drake, G. GRIN optics for multispectral infrared imaging. *Proc. SPIE* **2015**, *9451*, 94511P.
92. Mizrahi, V.; Delong, K.; Stegeman, G.; Saifi, M.; Andrejco, M. 2-Photon Absorption as a Limitation to All-Optical Switching. *Opt. Lett.* **1989**, *14*, 1140–1142. [CrossRef] [PubMed]
93. Devilliers, C.; Kroedel, M. CESIC: A new technology for lightweight and cost effective space instrument structures and mirrors. *SPIE Proc.* **2005**, *5868*, 58680F.
94. Mirov, S.B.; Fedorov, V.V.; Martyshkin, D.; Moskalev, I.S.; Mirov, M.; Vasilyev, S. Progress in Mid-IR Lasers Based on Cr and Fe-Doped II-VI Chalcogenides. *IEEE J. Sel. Top. Quantum Electron.* **2015**, *21*, 1601719. [CrossRef]
95. Martyshkin, D.V.; Goldstein, J.T.; Fedorov, V.V.; Mirov, S.B. Crystalline Cr^{2+}:ZnSe/chalcogenide glass composites as active mid-IR materials. *Opt. Lett.* **2011**, *36*, 1530–1532. [CrossRef] [PubMed]
96. Karaksina, E.V.; Shiryaev, V.S.; Ketkova, L.A. Preparation of composite materials for fiber optics based on chalcogenide glasses containing ZnS(ZnSe):Cr(2+) crystals. *J. Non-Cryst. Solids* **2013**, *377*, 220–224. [CrossRef]
97. Labadie, L.; Abel-Tiberini, L.; LeCoarer, E.; Vigreux-Bercovici, C.; Arezki, B.; Barillot, M.; Broquin, J.; Delboulbe, A.; Kern, P.; Kirschner, V.; et al. Recent progress in mid-infrared integrated optics for nulling interferometry. *SPIE Proc.* **2006**, *6268*, 62682E.
98. O'Donnell, M.D.; Seddon, A.B.; Furniss, D.; Tikhomirov, V.K.; Rivero-Baleine, C.; Ramme, M.; Stegeman, R.; Stegeman, G.; Richardson, K.; Stolen, R.; et al. Tellurite and fluoro-tellurite glasses for fiberoptic Raman amplifiers: Glass characterization, optical properties, Raman gain, preliminary fiberization and fiber characterization. *J. Am. Ceram. Soc.* **2007**, *90*, 1448–1457. [CrossRef]
99. O'Donnell, M.D.; Richardson, K.; Stolen, R.; Rivero-Baleine, C.; Cardinal, T.; Couzi, M.; Furniss, D.; Seddon, A.B. Raman gain of selected tellurite glasses for high power IR fiber lasers calculated from spontaneous scattering spectra. *Opt. Mater.* **2008**, *30*, 946–951. [CrossRef]
100. Wang, T.; Venkatram, N.; Gosciniak, J.; Cui, Y.; Qian, G.; Ji, W.; Tan, D. Multi-photon absorption and third-order nonlinearity in silicon at mid-infrared wavelengths. *Opt. Express* **2013**, *21*, 32192–32198. [CrossRef] [PubMed]

101. Bristow, A.; Rotenberg, N.; van Driel, H. Two-photon absorption and Kerr coefficients of silicon for 850–2200 nm. *Appl. Phys. Lett.* **2007**, *90*, 191104. [CrossRef]
102. Kato, T.; Suetsugu, Y.; Takagi, M.; Sasaoka, E.; Nishimura, M. Measurements of the nonlinear refractive index in optical fiber by the cross-phase-modulation method with depolarized pump light. *Opt. Lett.* **1995**, *20*, 988–990. [CrossRef] [PubMed]
103. Gholami, F.; Zlatanovic, S.; Simic, A.; Liu, L.; Borlaug, D.; Alic, N.; Nezhad, M.; Fainman, Y.; Radic, S. Third-order nonlinearity in silicon beyond 2350 nm. *Appl. Phys. Lett.* **2011**, *99*, 081102. [CrossRef]